PHYSICS

Ultrafast dissolution and creation of bonds in IrTe$_2$ induced by photodoping

Shin-ichiro Ideta[1,2]*[†], Dongfang Zhang[1]*[‡], Arend G. Dijkstra[1,3], Sergey Artyukhin[4], Sercan Keskin[1§], Roberto Cingolani[4], Takahiro Shimojima[2], Kyoko Ishizaka[2], Hiroyuki Ishii[5], Kazutaka Kudo[5], Minoru Nohara[5], R. J. Dwayne Miller[1,6¶]

The observation and control of interweaving spin, charge, orbital, and structural degrees of freedom in materials on ultrafast time scales reveal exotic quantum phenomena and enable new active forms of nanotechnology. Bonding is the prime example of the relation between electronic and nuclear degrees of freedom. We report direct evidence illustrating that photoexcitation can be used for ultrafast control of the breaking and recovery of bonds in solids on unprecedented time scales, near the limit for nuclear motions. We describe experimental and theoretical studies of IrTe$_2$ using femtosecond electron diffraction and density functional theory to investigate bonding instability. Ir-Ir dimerization shows an unexpected fast dissociation and recovery due to the filling of the antibonding d$_{xy}$ orbital. Bond length changes of 20% in IrTe$_2$ are achieved by effectively addressing the bonds directly through this relaxation process. These results could pave the way to ultrafast switching between metastable structures by photoinduced manipulation of the relative degree of bonding in this manner.

INTRODUCTION

The study of interactions among different degrees of freedom strongly coupled to the lattice is a crucial key for elucidating and manipulating material properties (1). The mechanism of structural phase transitions with the modulation of the electron density and the associated periodic lattice distortions (PLDs) represent an especially challenging issue for elucidating cooperative phenomena (2–5). IrTe$_2$ is of particular interest to survey the relationship between structural phase transitions and orbital ordering in the presence of strong spin-orbit coupling (6–12). IrTe$_2$ is a quasi–two-dimensional layered system, which undergoes a first-order structural transition between two crystalline phases at 260 K (12). The conduction electron density becomes modulated in a complex way, and modifying forces among the ions and generating PLDs with the bond lengths shortened: Ir-Ir and Te-Te bond lengths in the low-temperature (LT) phase decrease by 20 and 10%, respectively, compared with those in the high-temperature (HT) phase (13–17). This is due to bond formations, observed as the formation of in-plane Ir dimers and/or polymerization of Te chains (12, 13, 15) and accompanied by orbital/charge ordering observed by core-level photoemission spectroscopy (18, 19).

According to angle-resolved photoemission spectroscopy and density functional theory (DFT) studies (13, 16), the electronic structure of IrTe$_2$ near the Fermi level (E_F) shows a multi-orbital system consisting of Ir 5d and Te 5p and preserves its metallic properties in both LT and HT phases. In the LT phase, the density of states (DOS) at the bottom of the conduction band has a large contribution from Ir t$_{2g}$ orbitals, and the d$_{xy}$ orbital is expected to play an important role in the structural phase transition and stabilization of the LT phase (13, 17). Dimerization in IrTe$_2$ is quite a special example among phase transitions exhibited in transition metal dichalcogenides, in contrast to the well-known charge density wave (CDW) type transition, resulting in an energy gap formation at E_F in many other transition metal dichalcogenides and rare earth tellurides (20–22). Although there is no clear evidence of the CDW gap in IrTe$_2$ below the transition temperature (10, 15, 16), the suppression of DOS (pseudogap) is observed, similar to that in high-T_c cuprate superconductors (15, 16, 23). The phase transition toward LT in IrTe$_2$ has been suggested to originate in intralayer Ir-Ir dimers, which compete against the interlayer Te-Te bonds (9, 12). Besides, strong spin-orbit interactions appear to destabilize Ir dimers and possibly influence the structural phase transition temperature in IrTe$_2$ (11, 13, 18). These experimental results suggest that the orbital and/or charge ordering in IrTe$_2$ is different from that in the conventional CDW induced by Fermi surface nesting and momentum-dependent electron-phonon coupling (16).

Femtosecond time-resolved techniques "light up" the various active degrees of freedom by abruptly modulating the electronic distribution while mostly preserving the energy transfer mechanism and coupling strengths among electron, spin, and lattice subsystems (24, 25). While extensive experiments in IrTe$_2$ have been performed (6–19), time-resolved experiments have not been demonstrated as yet. Here, we investigated the structural dynamics of PLD in 20- to 100-nm-thick, free-standing slices of single-crystal IrTe$_2$ (see the Supplementary Materials). The present ultrafast pump-probe experiment operates on the natural time scale of strongly coupled electronic and lattice degrees of freedom in IrTe$_2$ and allows an unprecedented insight into the physics underlying these complex orderings.

[1]Max Planck Institute for the Structure and Dynamics of Matter, and Hamburg Center for Ultrafast Imaging, Luruper Chaussee 149, 22761 Hamburg, Germany. [2]Quantum-Phase Electronics Center, Department of Applied Physics, University of Tokyo, Tokyo 113-8656, Japan. [3]School of Chemistry and School of Physics and Astronomy, University of Leeds, Leeds LS2 9JT, UK. [4]Italian Institute of Technology, Via Morego, 30, 16163 Genova, Italy. [5]Research Institute for Interdisciplinary Science, Okayama University, Okayama 700-8530, Japan. [6]Departments of Chemistry and Physics, 80 St. George Street, University of Toronto, Toronto, Ontario M5S 3H6, Canada.
*These authors contributed equally to this work.
†Present address: Institute for Molecular Science (IMS), Okazaki 444-8585, Japan.
‡Present address: Deutsches Elektronen-Synchrotron DESY, Notkestraße 85, 22607 Hamburg, Germany.
§Present address: INM, Leibniz Institute for New Materials, D-66123 Saarbrücken, Germany.
¶Corresponding author. Email: dwayne.miller@mpsd.mpg.de

RESULTS

We performed femtosecond electron diffraction (FED) experiments in the transmission geometry along the c axis in both HT (300 K)

and LT (at ~200 K) phases. Figure 1 shows the background-subtracted electron diffraction pattern on 40-nm-thick $IrTe_2$ in the HT and LT phases, respectively. In the HT phase, the obvious electron diffraction patterns with the sixfold symmetry of the trigonal structure are observed. In the LT phase, the sequence of four weak superlattice peaks (SLs) highlighted by the arrows is visible between two Bragg peaks (BPs).

The time evolution of the relative intensity change of the diffraction signal is shown in Fig. 2 in the vicinity of BP and SL following photoexcitation by an optical pump pulse. Relative intensity changes from a BP and a nearest-neighboring SL are observed, as shown in Fig. 2 (A to D) (see also fig. S3). The corresponding lattice dynamics of the relative change in the Bragg peak ($\Delta I_{Bragg}/I_{Bragg}$), superlattice peak ($\Delta I_{SL}/I_{SL}$), and inelastic background ($\Delta I_{BG}/I_{BG}$) are plotted as functions of optical delay time in Fig. 2F. The intensity of SL is suppressed by ~13% on time scales of ~200 and 300 fs for 400- and 800-nm pump pulses, respectively, where the data are fit by two exponential decays. The decrease of $\Delta I_{SL}/I_{SL}$ and the accompanying increase of $\Delta I_{Bragg}/I_{Bragg}$ illustrate a cooperative behavior, indicating that the optically induced
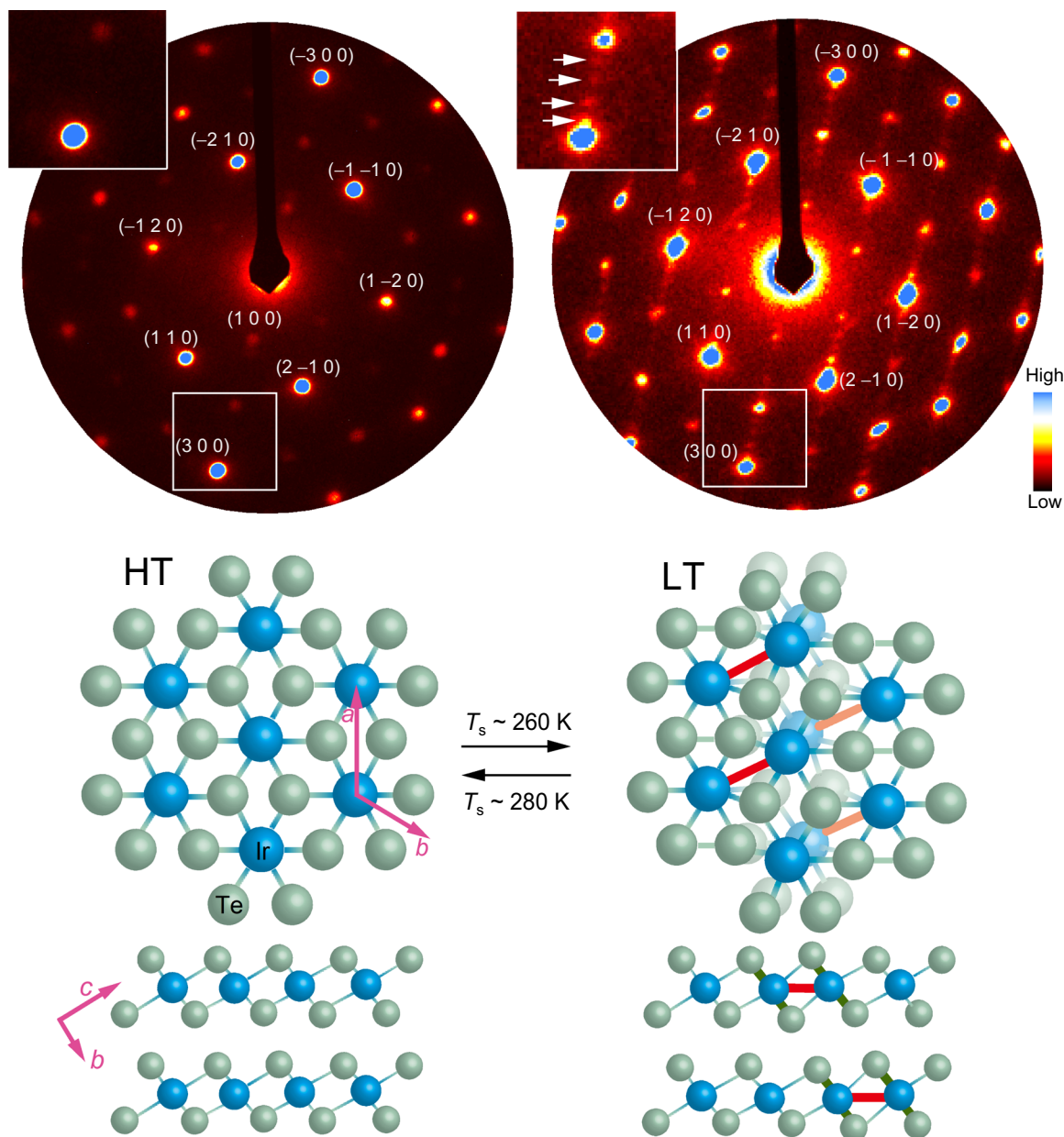

Fig. 1. Static electron diffraction image of $IrTe_2$ obtained by ultrahigh acceleration voltage 128-kV electron pulse. The upper panels are the electron diffraction obtained at 300 K (HT phase) and ~200 K (LT phase). The Miller indices (h k l) are also shown. Magnified view of the diffraction intensity (*I*) near the bright BP (see the white box in the upper panels) is also shown as an inset. The symmetry breaking, which corresponds to the presence of superlattices, is observed in the LT phase, as shown by arrows, and indicates the existence of a structural phase transition with modulation wave vectors q of (1/5, 0, 1/5) due to Ir-Ir dimerization and Te-Te polymerization (*7*, *9*, *13*). The bottom panels are the schematic illustration of $IrTe_2$ layers at the HT and LT phases. The HT phase observed at room temperature is formed by hexagonally arranged iridium (Ir) atoms, sandwiched by two tellurium (Te) layers coordinating the central Ir atom in an octahedral arrangement (*7*). In the LT phase, the structural change is associated with the phase transition at T_s ~ 260 K in combination with Ir-Ir (red line) and Te-Te (green line) dimerization with cooling from room temperature.
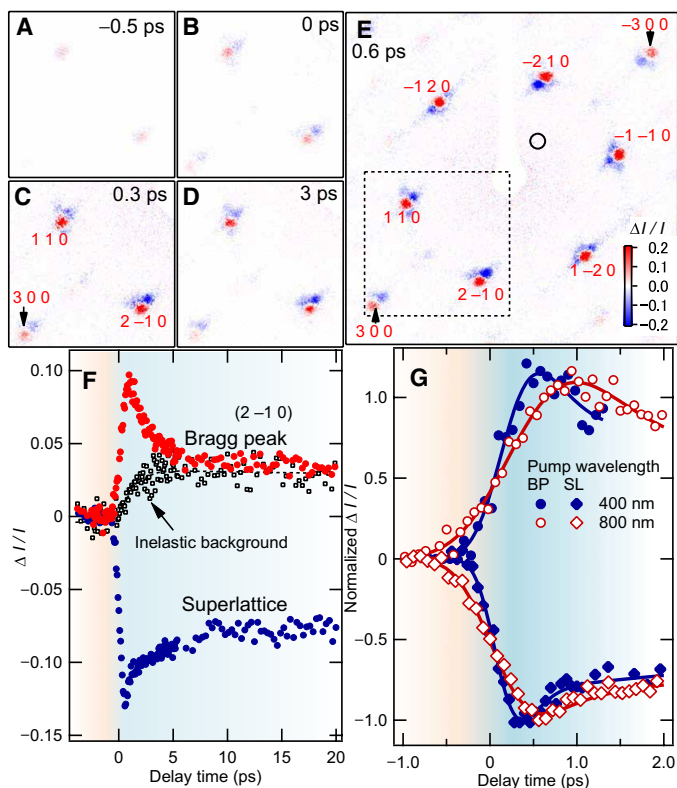
Fig. 2. Photoinduced time-dependent structural changes monitored by ultra-bright FED. (**A** to **D**) Differences of the diffraction patterns of the photoinduced and initial LT phases as a function of the delay time between the optical excitation and electron probe pulses, where the index at the HT phase is assigned. Note that red- and blue-colored scale denotes the increase and decrease of diffraction intensity after photoexcitation, respectively. (**E**) Wide view of the diffraction pattern subtracting of pump-probe and probe images after photoexcitation (+0.6 ps). (**F**) Relative intensity changes ($\Delta I/I$) for selected BPs and SLs. The intensity of BP from the host lattice is multiplied by two to see more clearly, and the fast dynamical processes are shown in (G). The excitation fluence was ~0.55 mJ/cm². The sample was photoexcited by 50-fs, 800-nm optical pulses at a repetition rate of 1 kHz. (**G**) Fast dynamical processes taken by 400- and 800-nm pump pulses, as indicated. Exponential fitting takes into account the electron and pump pulse duration with an error function as a guide to the eye. For $\Delta I_{SL}/I_{SL}$ ($\Delta I_{Bragg}/I_{Bragg}$), $\tau_{1,FED}$ ~ 200 fs (230 fs) and 300 fs (500 fs) for 400- and 800-nm pump, respectively.

redistribution of electron density decreases PLD and optimizes the symmetry of the crystal structure due to the structural phase transition. The suppression of PLD also increases the scattering of the host lattice into the Bragg reflection, as indicated by the increase (~10%) of $\Delta I_{Bragg}/I_{Bragg}$.

The electron-electron scattering arises on a much faster time scale compared with the electron-phonon scattering, and the lattice reaches a thermal equilibrium in the longer time scale compared with the electron-electron scattering, which allows one to disentangle different scattering mechanisms. There are two factors contributing to dimer dissolution: the population of the electronic excited state that induces the repulsion between Ir atoms forming the dimer, and the electron-phonon coupling inducing a higher effective lattice temperature that favors increased entropy. In the following, we refer to those contributions leading to dimer destabilization as the electronic contribution and thermal contribution, respectively. With further electron-electron and electron-phonon scattering, both the BPs and SLs start to recover,

accompanied by the increase of $\Delta I_{BG}/I_{BG}$ estimated from the area indicated by the black circle in Fig. 2E. PLD recovers because of the formation of the in-plane Ir-Ir displacement with dimerization.

Another noteworthy feature of the data shown in Fig. 2 (F and G) is the apparent faster recovery of $\Delta I_{SL}/I_{SL}$ between 0.5 and 1 ps. A minimum in I_{SL} is the time delay of 500 fs followed by a quick recovery on a time scale of $\tau_{1,FED}$ ~200 fs (400-nm pump) from that point, indicating an extra contribution from the electronic subsystem. This implies that the electrons relevant to the orbital ordering in the LT phase abruptly release their energy to the lattice via phonon emission. We attributed this intriguing phenomenon to the excitation of the d_{xy} antibonding state within a dimer verified by DFT to be discussed further below. Thus, the dynamical process after photoexcitation is described by several steps with different characteristic time scales: First, electrons in the bulk are photoexcited to the unoccupied state, especially the d_{xy} antibonding state, covering the characteristic energy of 0.26 eV above E_F as we show later and the dimerization breaks. Second, the dimerization starts to recover when the occupation of the electron in the d_{xy} antibonding state is reduced with the thermalization of hot electrons via electron-electron scattering ($\tau_{1,FED}$), and their subsequent cooling via the electron-phonon interaction. This leads to the thermal equilibrium of electrons and specific phonons on a time scale of $\tau_{2,FED}$ ~5 ps.

DISCUSSION

To obtain a better understanding of the process, we have used DFT to calculate the energy difference between the dimerized and nondimerized states ($\Delta E = E_{dimer} - E_{nondimer}$) for several electronic equilibrium temperatures. Because of fast electron-electron scattering, the electron system thermalizes rapidly, and we can approximate it with a Fermi-Dirac distribution with a certain elevated temperature from ambient. At LTs (region 1 of Fig. 3A), the system has two energy minima at the Ir-Ir distance of 3.1 and 3.9 Å, reflecting a stable state and a metastable state, respectively. The dimerized state has the lowest total energy ($\Delta E < 0$); therefore, the system stays in the dimerized state. When the electron temperature exceeds 3×10^3 K (0.26 eV), ΔE is reversed ($\Delta E > 0$): Only one minimum remains in the potential energy at an Ir-Ir distance of 3.9 Å, reflecting that the nondimerized state is stable and the dimers break (region 2). Inclusion of spin-orbit coupling makes the dimerized phase slightly less stable (see the Supplementary Materials). Surprisingly, the dimerized state becomes stable again when the electronic temperature is increased further above 2×10^4 K (1.72 eV), which implies the complexity of the occupation of the antibonding orbital and the filling of additional higher lying bonding orbitals in the excited states.

To strengthen this interpretation, we have also calculated the forces applied on the ions with fixed electron occupation. This calculation shows that when exciting electrons from the valence to the conduction band by adding 0.61 eV of energy, the Ir-Ir dimerized atoms move in opposite directions (Fig. 3B). This reflects dimer breaking in region 2. When looking at the DOS of those two atoms (see the Supplementary Materials), we observe that these electrons are mainly related to d orbitals that coincide with the above-mentioned d_{xy} antibonding state. This is a rather intriguing result and illustrates complex light-induced chemistry driven by ultrafast changes in the occupation of antibonding and bonding d orbitals. This electronic temperature range (3×10^3 to 2×10^4 K) also coincides with the width of the d_{xy} antibonding band predicted in (*13*, *17*).
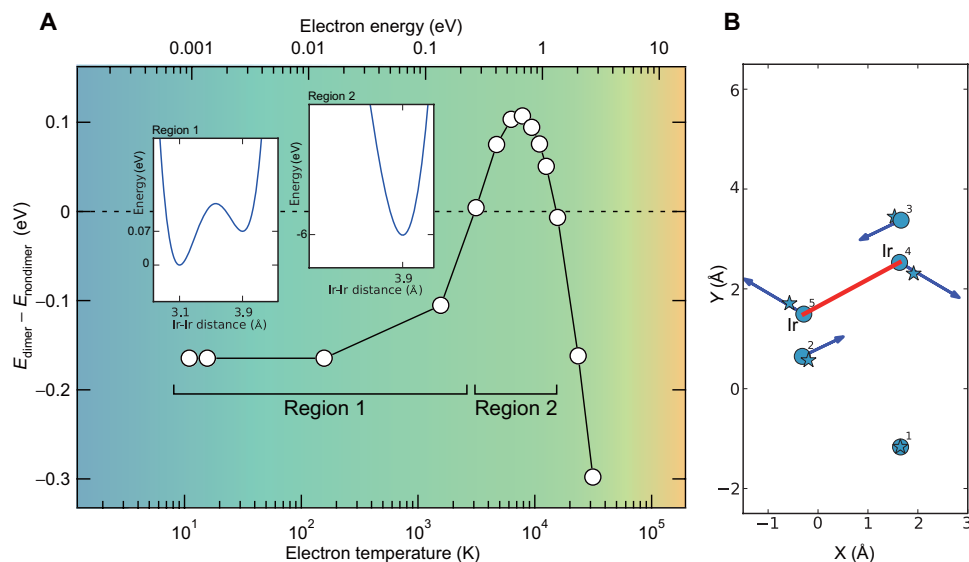
Fig. 3. DFT calculation using several temperatures. (**A**) Ir-Ir dimerization as a function of electronic temperature. Regions 1 and 2 indicate that the dimerized and non-dimerized phases are stable after the electron-electron interaction. The inset shows the potential energy change corresponding to regions 1 and 2. The shape of the energy surfaces is a cartoon, in particular, the height of the barrier at low electronic temperature was not calculated. (**B**) Calculated forces on Ir ions after optical excitation at 0.61 eV. The direction of the force is indicated by blue arrows. The representative dimerized structure is shown by circles and a red line, and the nondimerized structure is shown by stars. The result presented here is obtained from DFT calculations using the ideal crystal structure. The calculation using a relaxed structure at a certain electron temperature gives the same result. Calculations shown in the inset of (A) were done for electronic temperatures of 0.001 eV (LT) and 0.68 eV (intermediate temperature) and with DFT, as described in the Supplementary Materials. Both positions of the ion and the unit cell parameters were relaxed in the calculation.

Besides, when the electronic temperature is below 3×10^3 K, the probability of dimer breaking due to the electronic contribution is rather small, leaving the thermal contribution dominating. In line with the previous discussion of initial excitation, and subsequent electron thermalization and coupling to the lattice, the superlattice demonstrates a two-step recovery process: $\tau_{1,\text{FED}}$ that is mainly due to the electron occupation of the antibonding orbital and $\tau_{2,\text{FED}}$ that mainly arises from the electron-phonon coupling. However, the fast recovery of the $\Delta I_{\text{Bragg}}/I_{\text{Bragg}}$ is obscured by the simultaneous reduction of BP intensity resulting from the Debye-Waller effect at the same time scale of $\tau_{1,\text{FED}}$. Note that a suppression of $\Delta I_{\text{SL}}/I_{\text{SL}}$ on a long time scale (>10 ps) mainly comes from the Debye-Waller effect and thermally induced structural changes. Another plausible explanation is partial suppression/distortion from homogeneous thermalization of electrons. With the excitation used in the experiment (<1 mJ/cm^2), the electron temperature is very low with a homogeneous thermalization. The electron temperature cannot reach the d_{xy} antibonding state, and DFT calculation shows that with such an amount of electron temperature change, it is not enough to bring structural change toward the HT phase, and the forces applied to the dimerized ions are rather complex.

It is informative to compare the structural dynamics with those of the electronic subsystem via optical spectroscopy to elucidate the interaction between lattices and electrons. We have performed all-optical pump-probe spectroscopy measurements, reflecting the electronic state dynamics sensitive to the orbital occupations and DOS at E_F (26). The photoinduced reflectivity change (Fig. 4A) shows a rapid onset on the 150-fs time scale, followed by a fast recovery with a decay time of $\tau_{1,\text{opt}}$ ~200 fs and subsequent slower decay with a relaxation time of $\tau_{2,\text{opt}}$ ~10 ps. The short decay time scale is attributed to the energy transfer, implying that Ir 5d and Te 5p orbital orders (15) are partially dissolved, while the intermediate decay time scale indicates
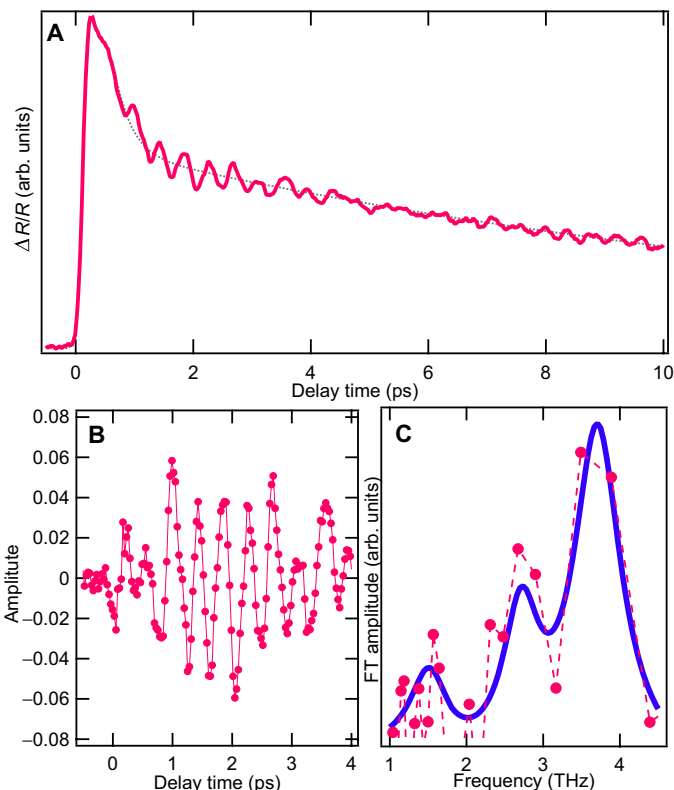

Fig. 4. Dynamics of the differential reflectivity change. (**A**) Transient reflectivity: relative intensity changes from a bulk sample at the LT phase ~200 K recorded at the excitation wavelength (800 nm, 100 fs) and fluence (1 mJ/cm^2). (**B**) Subtraction from the fitting curve to raw data of (A). (**C**) FTs of the transient reflectivity of (B). Dots are the result, and a curve as a guide to the eye is the fit of Lorentzians.
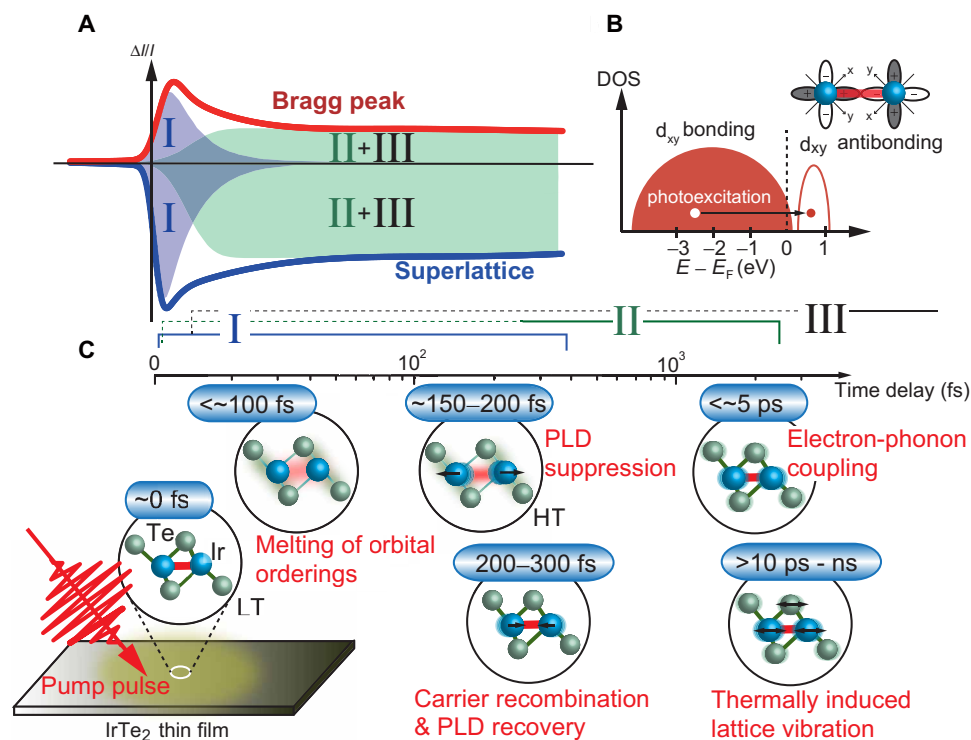
Fig. 5. Ultrafast photoinduced transient cooperative processes in IrTe₂. (**A**) Schematic lattice dynamics obtained from the present study. Component of I, II, and III corresponds to the dynamics of electron-electron, electron-lattice, and thermal relaxation. (**B**) Schematic DOS of the filled d_{xy} bonding and unoccupied antibonding states with photoexcitation process in the LT phase. The antibonding orbital is shown on the right. (**C**) Emerging time evolution of the real-space structure of the Ir-Te plane of IrTe₂ with the multi-orbital ordered state following photoexcitation with an intense optical pulse. For the characteristic time constant indicated by I, II, and III, the dashed and solid lines indicate the major and minor contributions from the interaction, respectively.

that hot electrons release the energy to the lattice via phonon emission and the lattice temperature abruptly increases. Figure 4C shows a Fourier transform (FT) of the oscillation after subtracting the non-oscillating transient spectrum shown in Fig. 4B. Three distinct peaks at 1.5, 2.6, and 3.8 THz seen in the spectrum correspond to wave numbers of 53, 86, and 126 cm^{-1}, respectively. These frequencies coincide with Raman modes with A_g and B_g symmetry in the LT phase (27) that can be coherently excited by the pump pulse. The decay $\tau_{1,\text{opt}}$ matches quite well with the present FED results and indicates that the fast electronic contribution is due to the filling of the d_{xy} antibonding orbital.

Figure 5 summarizes the transient photo-driven cooperative processes in IrTe₂. The present FED study reveals a dimer dissolution due to the population of the d_{xy} antibonding state. In IrTe₂, hot electrons excited to the d_{xy} antibonding state induce the breakup of Ir-Ir dimers, which quickly recover because of the reduction of the electron density in the d_{xy} antibonding state as the electrons thermalize and depopulate the antibonding state. Afterward, the electron-phonon interaction starts to dominate, and the lattice temperature increases near the HT phase. Thereby, the present study indicates that a specific lattice system is strongly coupled with the d_{xy} orbital order. A recently published study using FED and time-resolved angle-resolved photoemission spectroscopy (tr-ARPES) has reported a similar dynamical process in In-In bonds on the Si surface (25). To further corroborate our findings, tr-ARPES would be helpful for understanding the non-equilibrium physics of materials with strong electron-phonon interactions (28).

The combined experimental FED and optical and theoretical DFT studies have uncovered surprising lattice dynamics reflecting nuclear motions strongly coupled with the electronic subsystem. The present work demonstrates that the ultrafast manipulation of orbital orders (namely, ultrafast switching between dimerization and nondimerization) and electronic control of the specific lattice subsystem are possible. This new insight can be used to control the degree of bonding, not as in the quantum control sense, but by explicit use of the localized changes in electron density to affect control over the lattice potential by photoexcitation to manipulate the material properties through change in bond order. It paves the way to the controlled breaking and creation of bonds by the applied pulse sequences. A more controlled excitation that can exactly fill in the antibonding orbital will also make the manipulation of the dimers more efficient. Switching between metastable structures with different bonding patterns, such as graphite-diamond, following this approach, would be particularly exciting. This straightforward experimental method will be extended for surveying the mechanism and control of interesting physical properties that holds potential to lead materials science to exploit metastable states as pathways to new material properties.

MATERIALS AND METHODS
Single crystals of IrTe₂ were fabricated by the self-flux technique. IrTe₂ thin films (20 to 100 nm in thickness) for FED were obtained from an IrTe₂ bulk sample using a microtome (the thicknesses were determined by the microtome). The thin films sliced from the bulk

sample were dropped into distilled water, picked up by a loop, and put onto a Cu mesh for transmission electron microscopy (TEM; see also the Supplementary Materials) to obtain a good thermal contact. The thin films of IrTe$_2$ on the Cu mesh were set on a sample holder made of oxygen-free Cu for both FED and optical pump-probe experiments. For both experiments, a sample temperature of ~200 K was achieved using liquid N$_2$. We measured the sample temperature using a calibrated temperature sensor. The vacuum pressure was 10^{-6} Pa. We performed FED experiments using the fundamental (800 nm, 50 fs) output beam from a commercial Ti:sapphire laser system (Coherent). The fundamental laser pulse was split into two arms with a beam splitter for both pump and probe. A 266-nm laser beam was generated through the third harmonic generation and was directed onto a gold photocathode generating ultrashort electron pulses. Photoelectrons were finally accelerated to 128 kV by a dc electric field between the photocathode and anode plates. Diffracted and directly transmitted electrons were focused with the magnetic lens onto a 1:1 fiber-coupled charge-coupled device camera (Quad-RO 4320, Princeton Instruments) coated with a P20 phosphor scintillator. To investigate the effect of optical excitation on the structural dynamics in IrTe$_2$, we demonstrated DFT calculation using the projector-augmented wave formalism for core-valence partitioning, as implemented in the Quantum Espresso code (*29*). Details of the DFT calculation are given in the Supplementary Materials.

SUPPLEMENTARY MATERIALS

REFERENCES AND NOTES

1. H. Y. Hwang, Y. Iwasa, M. Kawasaki, B. Keimer, N. Nagaosa, Y. Tokura, Emergent phenomena at oxide interfaces. *Nat. Mater.* **11**, 103–113 (2012).
2. P. Beaud, S. L. Johnson, E. Vorobeva, U. Staub, R. A. De Souza, C. J. Milne, Q. X. Jia, G. Ingold, Ultrafast structural phase transition driven by photoinduced melting of charge and orbital order. *Phys. Rev. Lett.* **103**, 155702 (2009).
3. V. R. Morrison, R. P. Chatelain, K. L. Tiwari, A. Hendaoui, A. Bruhács, M. Chaker, B. J. Siwick, A photoinduced metal-like phase of monoclinic VO$_2$ revealed by ultrafast electron diffraction. *Science* **346**, 445–448 (2014).
4. M. Eichberger, H. Schäfer, M. Krumova, M. Beyer, J. Demsar, H. Berger, G. Moriena, G. Sciaini, R. J. D. Miller, Snapshots of cooperative atomic motions in the optical suppression of charge density waves. *Nature* **468**, 799–802 (2010).
5. S. K. Sundaram, E. Mazur, Inducing and probing non-thermal transitions in semiconductors using femtosecond laser pulses. *Nat. Mater.* **1**, 217–224 (2002).
6. H. Cao, B. C. Chakoumakos, X. Chen, J. Yan, M. A. McGuire, H. Yang, R. Custelcean, H. Zhou, D. J. Singh, D. Mandrus, Origin of the phase transition in IrTe$_2$: Structural modulation and local bonding instability. *Phys. Rev. B* **88**, 115122 (2013).
7. S. Pyon, K. Kudo, M. Nohara, Superconductivity induced by bond breaking in the triangular lattice of IrTe$_2$. *J. Phys. Soc. Jpn.* **81**, 053701 (2012).
8. G. L. Pascut, T. Birol, M. J. Gutmann, J. J. Yang, S.-W. Cheong, K. Haule, V. Kiryukhin, Series of alternating states with unpolarized and spin-polarized bands in dimerized IrTe$_2$. *Phys. Rev. B* **90**, 195122 (2014).
9. J. Dai, K. Haule, J. J. Yang, Y. S. Oh, S.-W. Cheong, W. Wu, Hierarchical stripe phases in IrTe$_2$ driven by competition between Ir dimerization and Te bonding. *Phys. Rev. B* **90**, 235121 (2014).
10. A. F. Fang, G. Xu, T. Dong, P. Zheng, N. L. Wang, Structural phase transition in IrTe$_2$: A combined study of optical spectroscopy and band structure calculations. *Sci. Rep.* **3**, 1153 (2013).
11. J. J. Yang, Y. J. Choi, Y. S. Oh, A. Hogan, Y. Horibe, K. Kim, B. I. Min, S.-W. Cheong, Charge-orbital density wave and superconductivity in the strong spin-orbit coupled IrTe$_2$:Pd. *Phys. Rev. Lett.* **108**, 116402 (2012).
12. Y. S. Oh, J. J. Yang, Y. Horibe, S.-W. Cheong, Anionic depolymerization transition in IrTe$_2$. *Phys. Rev. Lett.* **110**, 127209 (2013).
13. G. L. Pascut, K. Haule, M. J. Gutmann, S. A. Barnett, A. Bombardi, S. Artyukhin, T. Birol, D. Vanderbilt, J. J. Yang, S.-W. Cheong, V. Kiryukhin, Dimerization-induced cross-layer quasi-two-dimensionality in metallic IrTe$_2$. *Phys. Rev. Lett.* **112**, 086402 (2014).
14. T. Toriyama, M. Kobori, T. Konishi, Y. Ohta, K. Sugimoto, J. Kim, A. Fujiwara, S. Pyon, K. Kudo, M. Nohara, Switching of conducting planes by partial dimer formation in IrTe$_2$. *J. Phys. Soc. Jpn.* **83**, 033701 (2014).
15. Q. Li, W. Lin, J. Yan, X. Chen, A. G. Gianfrancesco, D. J. Singh, D. Mandrus, S. V. Kalinin, M. Pan, Bond competition and phase evolution on the IrTe$_2$ surface. *Nat. Commun.* **5**, 5358 (2014).
16. D. Ootsuki, Y. Wakisaka, S. Pyon, K. Kudo, M. Nohara, M. Arita, H. Anzai, H. Namatame, M. Taniguchi, N. L. Saini, T. Mizokawa, Orbital degeneracy and Peierls instability in the triangular-lattice superconductor Ir$_{1-x}$Pt$_x$Te$_2$. *Phys. Rev. B* **86**, 014519 (2012).
17. D. Mazumdar, K. Haule, J. J. Yang, G. L. Pascut, B. S. Holinsworth, K. R. O'Neal, V. Kiryukhin, S.-W. Cheong, J. L. Musfeldt, Optical evidence for bonding-antibonding splitting in IrTe$_2$. *Phys. Rev. B* **91**, 041105(R) (2015).
18. K.-T. Ko, H.-H. Lee, D.-H. Kim, J.-J. Yang, S.-W. Cheong, M. J. Eom, J. S. Kim, R. Gammag, K.-S. Kim, H.-S. Kim, T.-H. Kim, H.-W. Yeom, T.-Y. Koo, H.-D. Kim, J.-H. Park, Charge-ordering cascade with spin–orbit Mott dimer states in metallic iridium ditelluride. *Nat. Commun.* **6**, 7342 (2015).
19. H. S. Kim, S. Kim, K. Kim, B. I. Min, Y.-H. Cho, L. Wang, S.-W. Cheong, H. W. Yeom, Nanoscale superconducting honeycomb charge order in IrTe$_2$. *Nano Lett.* **16**, 4260–4265 (2016).
20. J. C. Petersen, S. Kaiser, N. Dean, A. Simoncig, H. Y. Liu, A. L. Cavalieri, C. Cacho, I. C. E. Turcu, E. Springate, F. Frassetto, L. Poletto, S. S. Dhesi, H. Berger, A. Cavalleri, Clocking the melting transition of charge and lattice order in 1*T*–TaS$_2$ with ultrafast extreme-ultraviolet angle-resolved photoemission spectroscopy. *Phys. Rev. Lett.* **107**, 177402 (2011).
21. F. Schmitt, P. S. Kirchmann, U. Bovensiepen, R. G. Moore, L. Rettig, M. Krenz, J.-H. Chu, N. Ru, L. Perfetti, D. H. Lu, M. Wolf, I. R. Fisher, Z.-X. Shen, Transient electronic structure and melting of a charge density wave in TbTe$_3$. *Science* **321**, 1649–1652 (2008).
22. T. Rohwer, S. Hellmann, M. Wiesenmayer, C. Sohrt, A. Stange, B. Slomski, A. Carr, Y. Liu, L. M. Avila, M. Kalläne, S. Mathias, L. Kipp, K. Rossnagel, M. Bauer, Collapse of long-range charge order tracked by time-resolved photoemission at high momenta. *Nature* **471**, 490–493 (2011).
23. H. Ding, T. Yokoya, J. C. Campuzano, T. Takahashi, M. Randeria, M. R. Norman, T. Mochiku, K. Kadowaki, J. Giapintzakis, Spectroscopic evidence for a pseudogap in the normal state of underdoped high-T_c superconductors. *Nature* **382**, 51–54 (1996).
24. G. Sciaini, R. J. D. Miller, Femtosecond electron diffraction: Heralding the era of atomically resolved dynamics. *Rep. Prog. Phys.* **74**, 096101 (2011).
25. T. Frigge, B. Hafke, T. Witte, B. Krenzer, C. Streubühr, A. Samad Syed, V. Mikšić Trontl, I. Avigo, P. Zhou, M. Ligges, D. von der Linde, U. Bovensiepen, M. Horn-von Hoegen, S. Wippermann, A. Lücke, S. Sanna, U. Gerstmann, W. G. Schmidt, Optically excited structural transition in atomic wires on surfaces at the quantum limit. *Nature* **544**, 207–211 (2017).
26. J. Hohlfeld, S.-S. Wellershoff, J. Güdde, U. Conrad, V. Jähnke, E. Matthias, Electron and lattice dynamics following optical excitation of metals. *Chem. Phys.* **251**, 237–258 (2000).
27. N. Lazarević, E. S. Bozin, M. Šćepanović, M. Opačić, H. Lei, C. Petrovic, Z. V. Popović, Probing IrTe$_2$ crystal symmetry by polarized Raman scattering. *Phys. Rev. B* **89**, 224301 (2014).
28. J. D. Rameau, S. Freutel, A. F. Kemper, M. A. Sentef, J. K. Freericks, I. Avigo, M. Ligges, L. Rettig, Y. Yoshida, H. Eisaki, J. Schneeloch, R. D. Zhong, Z. J. Xu, G. D. Gu, P. D. Johnson,

U. Bovensiepen, Energy dissipation from a correlated system driven out of equilibrium. *Nat. Commun.* **7**, 13761 (2016).

29. P. Giannozzi, S. Baroni, N. Bonini, M. Calandra, R. Car, C. Cavazzoni, D. Ceresoli, G. L. Chiarotti, M. Cococcioni, I. Dabo, A. Dal Corso, S. de Gironcoli, S. Fabris, G. Fratesi, R. Gebauer, U. Gerstmann, C. Gougoussis, A. Kokalj, M. Lazzeri, L. Martin-Samos, N. Marzari, F. Mauri, R. Mazzarello, S. Paolini, A. Pasquarello, L. Paulatto, C. Sbraccia, S. Scandolo, G. Sclauzero, A. P. Seitsonen, A. Smogunov, P. Umari, R. M. Wentzcovitch, QUANTUM ESPRESSO: A modular and open-source software project for quantum simulations of materials. *J. Phys. Condens. Matter* **21**, 395502 (2009).

30. K. Kim, S. Kim, K.-T. Ko, H. Lee, J.-H. Park, J. J. Yang, S.-W. Cheong, B. I. Min, Origin of first-order-type electronic and structural transitions in IrTe$_2$. *Phys. Rev. Lett.* **114**, 136401 (2015).

31. A. Dal Corso, Pseudopotentials periodic table: From H to Pu. *Comput. Mater. Sci.* **95**, 337–350 (2014).

32. H. Lei, K. Wang, M. Abeykoon, E. Bozin, J. B. Warren, C. Petrovic, Superconductivity in Ir$_{1-x}$Rh$_x$Te$_2$ ($0 \leq x \leq 0.3$). arXiv:1307.7029v1 (2013).

Citation: S.-i. Ideta, D. Zhang, A. G. Dijkstra, S. Artyukhin, S. Keskin, R. Cingolani, T. Shimojima, K. Ishizaka, H. Ishii, K. Kudo, M. Nohara, R. J. D. Miller, Ultrafast dissolution and creation of bonds in IrTe$_2$ induced by photodoping. *Sci. Adv.* **4**, eaar3867 (2018).